Geophysical Research Letters

RESEARCH LETTER
10.1029/2018GL081393

Key Points:
- Modeled trajectories to, and time of emergence of, an ice-free Arctic are modulated by concomitant shifts in Pacific Ocean variability
- Faster sea-ice loss during the shift from the negative to the positive phase of the Interdecadal Pacific Oscillation leads to earlier ice-free Arctic
- There is increased likelihood of accelerated Arctic sea-ice loss over the coming decades if current shift of Interdecadal Pacific Oscillation continues

Supporting Information:
- Supporting Information S1

Correspondence to:
J. A. Screen,
j.screen@exeter.ac.uk

Citation:
Screen, J. A., & Deser, C. (2019). Pacific Ocean variability influences the time of emergence of a seasonally ice-free Arctic Ocean. *Geophysical Research Letters*, *46*. https://doi.org/10.1029/2018GL081393

Received 21 NOV 2018
Accepted 4 FEB 2019
Accepted article online 5 FEB 2019

Pacific Ocean Variability Influences the Time of Emergence of a Seasonally Ice-Free Arctic Ocean

J. A. Screen[1] and **C. Deser**[2]

[1]Global Systems Institute and Department of Mathematics, University of Exeter, Exeter, Devon, UK, [2]Climate and Global Dynamics, National Center for Atmospheric Research, Boulder, CO, USA

Abstract The Arctic Ocean is projected to become seasonally ice-free before midcentury unless greenhouse gas emissions are rapidly reduced, but exactly when this could occur depends considerably on internal climate variability. Here we show that trajectories to an ice-free Arctic are modulated by concomitant shifts in the Interdecadal Pacific Oscillation (IPO). Trajectories starting in the negative IPO phase become ice-free 7 years sooner than those starting in the positive IPO phase. Trajectories starting in the negative IPO phase subsequently transition toward the positive IPO phase, on average, with an associated strengthening of the Aleutian Low, increased poleward energy transport, and faster sea-ice loss. The observed IPO began to transition away from its negative phase in the past few years. If this shift continues, our results suggest increased likelihood of accelerated sea-ice loss over the coming decades, and an increased risk of an ice-free Arctic within the next 20–30 years.

Plain Language Summary Manmade climate change is causing a rapid loss of Arctic sea ice. Summer Arctic sea ice is predicted to disappear almost completely by the middle of this century, unless emissions of greenhouse gases are rapidly reduced. The speed of sea-ice loss is not constant over time, however. Natural climate variability can add to the manmade decline, leading to faster sea-ice loss, or can subtract from the manmade decline, leading to slower sea-ice loss. In this study, we looked at how natural climate variability affects the timing of an ice-free Arctic. We found that a natural cycle called the Interdecadal Pacific Oscillation, or IPO for short, is particularly important. Arctic sea-ice loss is faster when the IPO is moving from its cold to warm phase and slower when the IPO is moving from its warm to cold phase. This is because variations in the IPO cause changes in atmospheric wind patterns, which alter the amount of heat that is transported into the Arctic. Observations show that the IPO started to shift from its cold to warm phase in the past few years. If this shift continues, our results suggest that there is an increased chance of accelerated sea-ice loss over the coming decades.

1. Introduction

Arctic sea-ice cover has declined in recent decades across all calendar months (Kay et al., 2011; Stroeve & Notz, 2018). This decline directly follows the rise in global mean surface temperature (Mahlstein & Knutti, 2012; Niederdrenk & Notz, 2018; Rosenblum and Eisenmann, 2016, 2017) and anthropogenic CO_2 emissions (Notz & Stroeve, 2016). The Arctic will become seasonally ice-free before midcentury unless greenhouse gas emissions are rapidly reduced (Notz & Stroeve, 2018; Stroeve et al., 2012) and even the strictest emissions reduction targets may be insufficient to prevent occasional ice-free summers (Jahn, 2018; Screen, 2018; Screen & Williamson, 2017; Sigmond et al., 2018). An ice-free summer could conceivably occur within the next two decades (Jahn, 2018).

Superimposed on the long-term Arctic sea-ice decline is the year-to-year and decade-to-decade variability due to internal climate variability (Day et al., 2012; Kay et al., 2011; Swart et al., 2015; Zhang, 2015). Internal variability may be responsible for 40–50% of Arctic sea-ice decline observed over the past 37 years (Ding et al., 2019). Looking to the future, internal variability exerts a strong influence on the timing of the first ice-free summer (Jahn, 2018; Jahn et al., 2016). For a given greenhouse gas emissions scenario, this timing can vary by 20 years due to internal variability alone (Jahn et al., 2016). This means that it is possible, although less likely, for an ice-free Arctic to occur earlier in a low emissions scenario than a high emissions scenario (Jahn, 2018). Despite recognition of the important role of internal variability in the timing of an

ice-free Arctic, the physical mechanisms responsible have not been explored in much detail. There is growing evidence that tropical decadal variability can influence sea-ice trends in both hemispheres (Ding et al., 2017, 2019; Meehl, Arblaster, et al., 2016; Meehl et al., 2018; Purich et al., 2016; Schneider & Deser, 2017). Wettstein and Deser (2014) showed that internal variability is an important contributor to near-term projections of Arctic sea-ice extent. Higher rates of summer ice loss were found to be related to large-scale atmospheric circulation anomalies, including a Rossby wave train from the tropical Pacific. However, to our knowledge, our study is the first to specifically consider the role of tropical decadal variability in modulating the time of emergence of a seasonally ice-free Arctic.

2. Data and Methods

In this study, our primary tool for exploring Arctic sea-ice variability is the Community Earth System Model version 1 (CESM1) Large Ensemble (CESM1-LE; Kay et al., 2015). The CESM1-LE consists of 40 parallel simulations covering the years 1920 to 2100. Each individual simulation, referred to hereafter as an ensemble member, is performed with the same model version and with the same external forcing (e.g., greenhouse gas concentrations, ozone, aerosols, and land use). External forcing follows observed values from 1920 to 2005 and then the Representative Concentration Pathway 8.5 (RCP8.5) from 2006 to 2100. Representative Concentration Pathway 8.5 is a high-end emissions scenario, which in this model leads to global-average surface warming of 2 °C, relative to preindustrial, in approximately year 2040 and ~5 °C warming by 2100 (Kay et al., 2015). Ensemble members only differ from each other in their initial atmospheric conditions (through a round-off level perturbation to atmospheric temperature), which ensures that each member has a unique time sequence of internal (unforced) climate variability. More details can be found in Kay et al. (2015). We also make use of an 1800-year CESM1 control run with constant year 1850 external forcing. To document the observed changes, we use the satellite record of Arctic sea-ice extent provided by the National Snow and Ice Data Center (Fetterer et al., 2017) for the period 1979–2017 and version 5 of the NOAA Extended Reconstructed Sea Surface Temperature data set for the period 1880–2017 (Huang et al., 2017).

We use the common definitions for Arctic sea-ice extent and for an ice-free Arctic, which are the total area of grid cells with a sea-ice concentration of at least 15% and sea-ice extent below 1×10^6 km^2, respectively. The Interdecadal Pacific Oscillation (IPO) index is defined from 11-year running mean annual-mean SST using the tripole index of Henley et al. (2015). Before calculating the IPO index, we removed the externally forced response to retain only the internal variability. For CESM1-LE, we subtracted the ensemble-mean SST from each ensemble member, for each year and at each grid point. For the NOAA Extended Reconstructed Sea Surface Temperature, we removed an estimate of the forced response defined as the 137-year (1880–2017) linear trend at each grid point. The Aleutian Low (AL) index is defined by the area-averaged mean sea level pressure over North Pacific (160–220°E, 30–65°N), consistent with the North Pacific Index of Trenberth and Hurrell (1994). Here we have reversed the sign of the AL index such that positive values correspond to a strengthened AL (i.e., reduced mean sea level pressure). The IPO and AL indices were normalized by removing their mean and dividing by their standard deviation. Unless otherwise stated, all analyses were conducted using 11-year running means.

3. Results

3.1. Trajectories to an Ice-Free Arctic

Figure 1a shows observed September sea-ice extent (SSIE) from 1980 to 2017 and simulated SSIE from 1980 to 2060, the latter from the CESM1-LE. Since an ice-free Arctic will emerge first in September (Jahn, 2018), if at all, we focus solely on this month. The ensemble-mean depicts the emergence of ice-free conditions in 2046. Note that this is when the 11-year running mean SSIE first falls below 1×10^6 km^2, which provides an indication of when frequent ice-free Septembers emerge; occasional ice-free Septembers are simulated sooner than this. Note that the terminology “time of emergence” is often used to describe when anthropogenic climate change becomes separable from internal climate variability (Hawkins & Sutton, 2012); however, we use this wording to simply denote the time when the 11-year running mean SSIE first falls below 1×10^6 km^2.

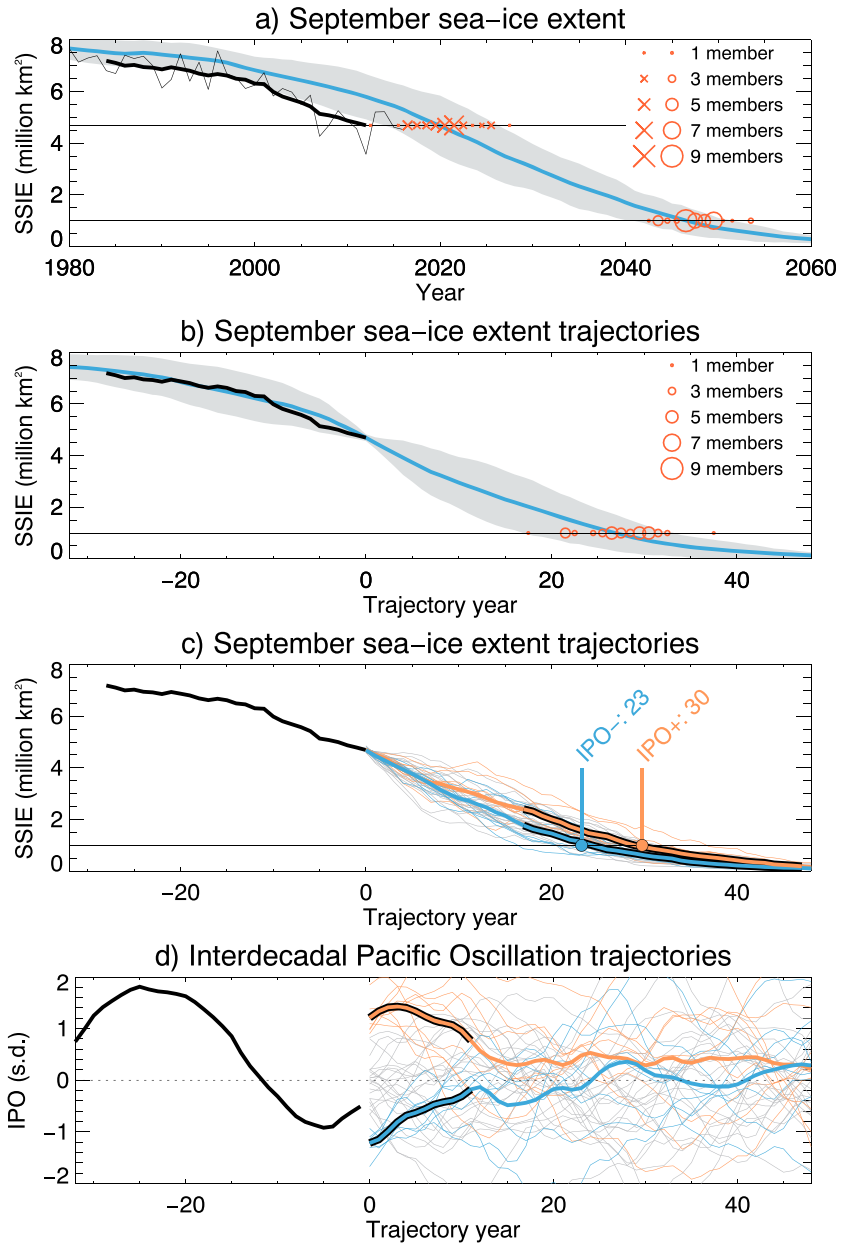

Figure 1. Arctic sea-ice projections. (a) September sea-ice extent (SSIE) in observations and the Community Earth System Model version 1 Large Ensemble (CESM1-LE). The observed sea-ice extent is shown with a thin black curve and its 11-year running mean with a thick black curve. The simulated ensemble-mean 11-year running mean is shown by the blue curve and the 2σ (95%) range by gray shading. Horizontal lines denote the observed present-day (2007–2017 average) SSIE (4.7×10^6 km^2) and the common threshold for an ice-free Arctic (1×10^6 km^2). Orange crosses and circles denote the year when each ensemble member is closest to 4.7×10^6 km^2 and the year when they first fall below 1×10^6 km^2, respectively, and their size denotes the number of members meeting these criteria in a single year. (b) As (a), but the for SSIE trajectories. (c) SSIE trajectories, categorized by the Interdecadal Pacific Oscillation (IPO) index in year 0. Thin blue, gray, and orange lines denote trajectories starting in negative IPO ($< -0.9\sigma$), neutral IPO ($> -0.9\sigma$ and $<0.9\sigma$) and positive IPO ($>0.9\sigma$), respectively. The thicker orange and blue lines denote the average of the positive and negative IPO cases, respectively, and have a black border where they are statistically different from each other ($p < 0.05$). Filled circles show when the average trajectories first become ice-free. (d) As (c), but for the IPO trajectories. Note that the *x* axis in (b)–(d) is the trajectory year and not the calendar year.

In this study we are primarily concerned with the rapidity of the transition from the present-day sea-ice state (defined as the 11-year period 2007–2017) to ice-free conditions. Figure 1a (specifically, the crosses) shows that some ensemble members reach the present-day observed SSIE sooner than other ensemble members. To account for this, in each ensemble member we identified the year when the 11-year running-mean SSIE most closely matches the observed SSIE for the period 2007–2017; we then use this year as the starting point (denoted year 0) for our forward trajectory analysis. This procedure yielded 40 SSIE trajectories, which all start from approximately the same value and are unbiased relative to recent observations. The same starting points were used to calculate corresponding trajectories for other variables. These starting points (crosses in Figure 1a) are later than 2007–2017, which is a reflection of the overestimation of SSIE in CESM1-LE.

The ensemble-mean SSIE trajectory, which represents the best estimate of the externally forced response, reaches ice-free conditions in year 27 (Figure 1b). The onset date of an ice-free Arctic ranges from year 17 to year 37 across the ensemble members. This 20-year range due to internal variability is consistent with large ensembles from other climate models (Jahn et al., 2016). Looking backward in time, the ensemble-mean SSIE trajectory captures well the observed sea-ice evolution. Thus, by considering simulated trajectories, as supposed to the raw model output, we circumvent the issue of a small SSIE bias (relative to many CMIP5 models, see e.g., Stroeve et al., 2012) in CESM1-LE (Figure 1a).

Figure 1b suggests that according to this model and emissions scenario, ice-free Septembers could occur within two decades from now. Previous studies have suggested that regional sea-ice cover may be predictable on this timescale (Germe et al., 2014; Guemas et al., 2016; Koenigk et al., 2012; Yeager et al., 2015; Yang et al., 2016). Here we investigate whether the current phase of slowly evolving ocean variability could shift the odds in favor of an earlier or later emergence of ice-free conditions. We search for evidence of this in CESM1-LE by correlating the time of emergence of an ice-free Arctic in each trajectory against the 11-year running-mean SST in the first year (hereafter termed year 0) of each trajectory (Figure 2a). This is an application of the so-called ensemble correlation (Wettstein & Deser, 2014), which seeks to explain how ensemble diversity in one variable is statistically related to ensemble spread in another variable. Figure 2a is constructed to show the SST pattern in year 0 that is associated with an earlier occurrence of ice-free conditions (i.e., the sign of the correlation is reversed). It reveals a significant relationship between the timing of an ice-free Arctic and Pacific Ocean SSTs. More specifically, an earlier emergence of ice-free conditions is linked to an SST anomaly pattern that bears strong resemblance to the negative phase of the IPO (supporting information Figure S1). The ensemble correlations (Figure 2a) imply that SSIE trajectories starting during the negative IPO phase become ice-free sooner than those starting during the positive IPO phase. Indeed, the IPO index in year 0 is a good predictor ($r = 0.52$; $p < 0.001$) of the timing of an ice-free Arctic (Figure 2b). We find no clear association between the timing of an ice-free Arctic and Atlantic Ocean SST in year 0 (Figure 2a).

3.2. Influence of the IPO

The IPO is a long-term oscillation of SST in the Pacific Ocean that can last from 10 to 30 years (Henley et al., 2015). During the negative phase, cool SST anomalies occur along the North Pacific coast of North America and warm SST anomalies in the interior North Pacific (supporting information Figure S1). This trend reverses during the positive IPO phase. The IPO has a similar surface ocean signature to the Pacific Decadal Oscillation (e.g., Figure 1a in Newman et al., 2016), but the IPO-related SST anomalies extend further into the South Pacific. Our choice to focus hereafter on the IPO, as opposed to other metrics of Pacific Ocean variability, reflects the strong hemispheric symmetry in Figure 2a and the high pattern correlation between Figure 2a and supporting information Figure S1b ($r = 0.9$ over the Indo-Pacific sector, 40°E–100°W, 70°N–70°S). The simulated IPO in CESM1 has a realistic spatial pattern and phase duration (supporting information Figure S1).

The influence of the IPO on the time of emergence of ice-free conditions is further shown in Figure 1c. Here we have split the SSIE trajectories into three categories (positive, neutral, and negative) depending on the IPO index in year 0. On average, SSIE trajectories starting in the negative IPO phase become ice-free 7 years sooner than those starting in the positive IPO phase (year 23 vs. year 30). Also, the trajectories that reach ice-free conditions earliest and latest start in the negative and positive IPO phase, respectively. By definition, the SSIE trajectories lie close to each other in year 0 and remain so for around 5 years but begin to diverge thereafter. The IPO positive and IPO negative average trajectories become statistically separable by year 17 and

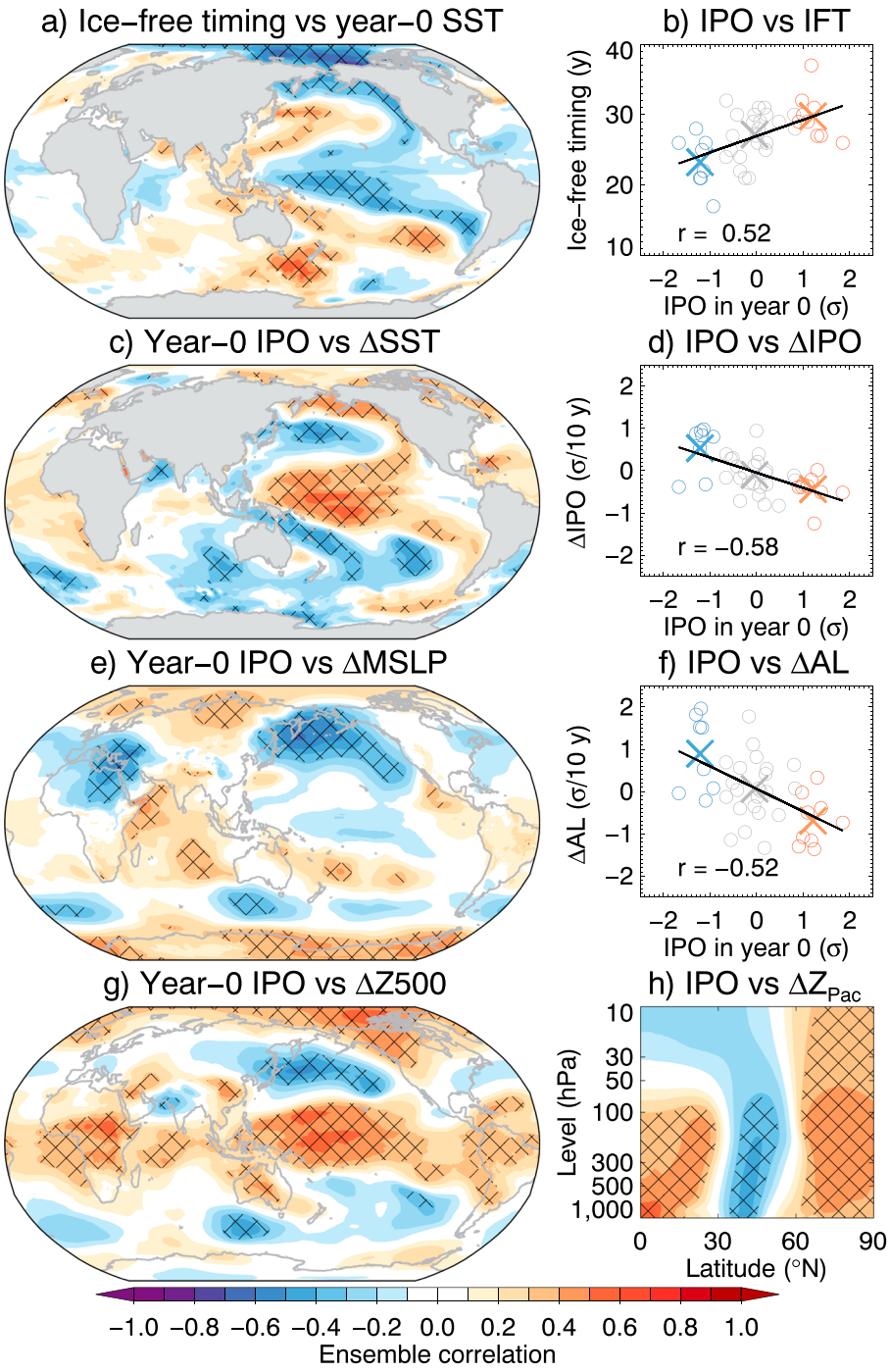

Figure 2. Internal climate variability linked to faster sea-ice loss. (a) Ensemble correlation between the time of emergence of an ice-free Arctic and annual-mean sea surface temperatures (SST) in year 0 of each trajectory. Black hatching shows statistical significance at the 95% confidence level ($p < 0.05$). The sign of the correlations has been reversed to display the pattern linked to an earlier emergence of ice-free conditions. (b) Relationship between the timing of ice-free conditions and the Interdecadal Pacific Oscillation (IPO) index in year 0. There are 40 circles, one per trajectory, which are colored according the IPO index in year 0 (as in Figure 1). The black line denotes the linear best fit, and the colored crosses show averages for the three IPO categories Ice-free timing (IFT). (c) As (a), but for the ensemble correlation between the IPO index in year 0 and the annual-mean SST trend in each trajectory. (d) As (b), but for the relationship between the IPO index in year 0 and the IPO trend. (e) As (c), but for the correlation between the IPO index in year 0 and the cold season (October–March) mean sea level pressure (MSLP) trend. (f) As (d), but for the relationship between the IPO index in year 0 and the cold season Aleutian Low (AL) trend. (g) As (c), but for the relationship between the IPO index in year 0 and the 500-hPa geopotential height (Z500) trend. (h) Ensemble correlation between the IPO index in year 0 and the geopotential height trend zonally averaged over the Pacific sector (Z_{Pac}). In (a, c, f, g), the sign of the correlations has been reversed to display the patterns linked to negative IPO in year 0.

remain distinct until year 40, by which time they have all become ice-free. Recall that the ensemble-mean trajectory, which is our best estimate of the forced response, first reaches an ice-free state in year 27.

Figure 1d shows corresponding trajectories for the IPO index, again categorized by the IPO index in year 0. By definition, the IPO positive and IPO negative average trajectories start from opposite IPO phases, and they remain significantly different from each other for over a decade. The two cases display large and opposite tendencies in the IPO in years 5–15. Note that we focus on the IPO tendency, rather than trajectory-mean IPO, because we are concerned with the forward evolution of SSIE from the baseline state in year 0. Trajectories starting from the negative IPO phase transition toward the positive IPO phase, on average, and trajectories starting from the positive IPO phase transition toward the negative IPO phase. It is during this period of rapid and opposite IPO change that the SSIE trajectories for IPO positive and negative cases begin to diverge. Trajectories transitioning from negative toward positive IPO show accelerated SSIE reduction compared to those transitioning from positive to negative IPO.

3.3. Physical mechanisms

To understand why the year-0 IPO index is a good predictor of the timing of an ice-free Arctic, we now explore associations between the year-0 IPO and subsequent trends in relevant variables, calculated over the period from year 0 until an ice-free Arctic is reached in each trajectory (i.e., for ensemble member 1, we take the linear trend from year 0 to year 30, when the 11-year running mean SSIE first falls below 1×10^6 km^2). Figure 2c shows that a negative IPO index in year 0 tends to be followed by SST trends that resemble the positive IPO phase. This is further borne out in Figure 2d, which shows that the year-0 IPO is a strong predictor ($r = -0.58$; $p < 0.001$) of the subsequent IPO trend. This can be understood in terms of the IPO trajectories (Figure 1d). More specifically, because of the oscillatory character of the IPO, negative IPO (associated with a colder Arctic) in year 0 is typically followed by a switch toward the positive (warmer Arctic) phase over the subsequent decade or two, and vice versa.

The year-0 IPO is also associated with subsequent trends in the cold season (October–March) atmospheric circulation. We focus on the cold season because this is when tropical-to-polar teleconnections are most active (e.g., Lee et al., 2009; Thomson & Vallis, 2018a, 2018b). Negative year-0 IPO is linked to subsequent decreasing mean sea level pressure trends in the North Pacific (Figure 2e), reflecting a strengthening of the AL. Indeed, the year-0 IPO is a good predictor ($r = -0.52$; $p < 0.001$) of the subsequent trend in the AL intensity (Figure 2f). This can be understood in terms of a transitioning IPO, with a shift toward the positive IPO phase coinciding with a strengthening of the AL. A strengthening AL is expected to increase lower atmospheric heat and moisture transport into the Pacific sector of the Arctic (Svendson et al., 2018; Tokinaga et al., 2017). Negative year-0 IPO is related to geopotential height trends that depict a planetary wave train from the tropical Pacific to the Arctic (Figures 2g and 2h). Positive height trends in the polar stratosphere are indicative of a weakening polar stratospheric vortex (Figure 2h). We find that connections between the year-0 IPO and midtropospheric circulation are broadly similar in the warm season (April–September) and in the cold season over lower latitudes but that the year-0 IPO is more closely related to circulation trends over the Arctic Ocean in the cold season (Supplementary Figure 2).

Locally within the Arctic, the year-0 IPO is strongly correlated with subsequent positive trends in cold season downward longwave radiation (DLR; Figure 3a) and near-surface air temperature (Figure 3b). In wintertime, Arctic surface temperatures are largely controlled by the DLR (Lee et al., 2017), and the DLR is to a large degree driven by horizontal moisture transport convergence (Gong et al., 2017). We therefore interpret the DLR and Arctic warming trends in Figure 3b to be partially driven by the IPO-related atmospheric circulation changes (Figure 2). In regions of sea-ice loss, the DLR will be enhanced by increased ocean-to-atmosphere heat and moisture fluxes (Screen & Simmonds, 2010). Warming, or more specifically fewer freezing degree days (Stroeve et al., 2018), may reduce sea-ice growth and contribute to reductions in sea-ice thickness across the Arctic (Figure 3c) and sea-ice concentration near the sea-ice edge (Figure 3d). Although thin ice grows faster than thick ice (Stroeve et al., 2018), this negative feedback is projected to weaken (Petty et al., 2018), implying a strengthening role of atmospheric controls on winter sea ice growth. Sea ice thinning and retreat of the sea-ice edge provide the preconditions for reduced SSIE. The cold season Arctic-mean sea-ice thickness reduction is very highly correlated ($r = 0.86$; $p < 0.001$) with SSIE loss across the ensemble (Figure 3e). Simulated sea-ice growth and melt rates provide further evidence of IPO-related preconditioning. Winter growth rates and summer melt rates are lower in trajectories starting in the

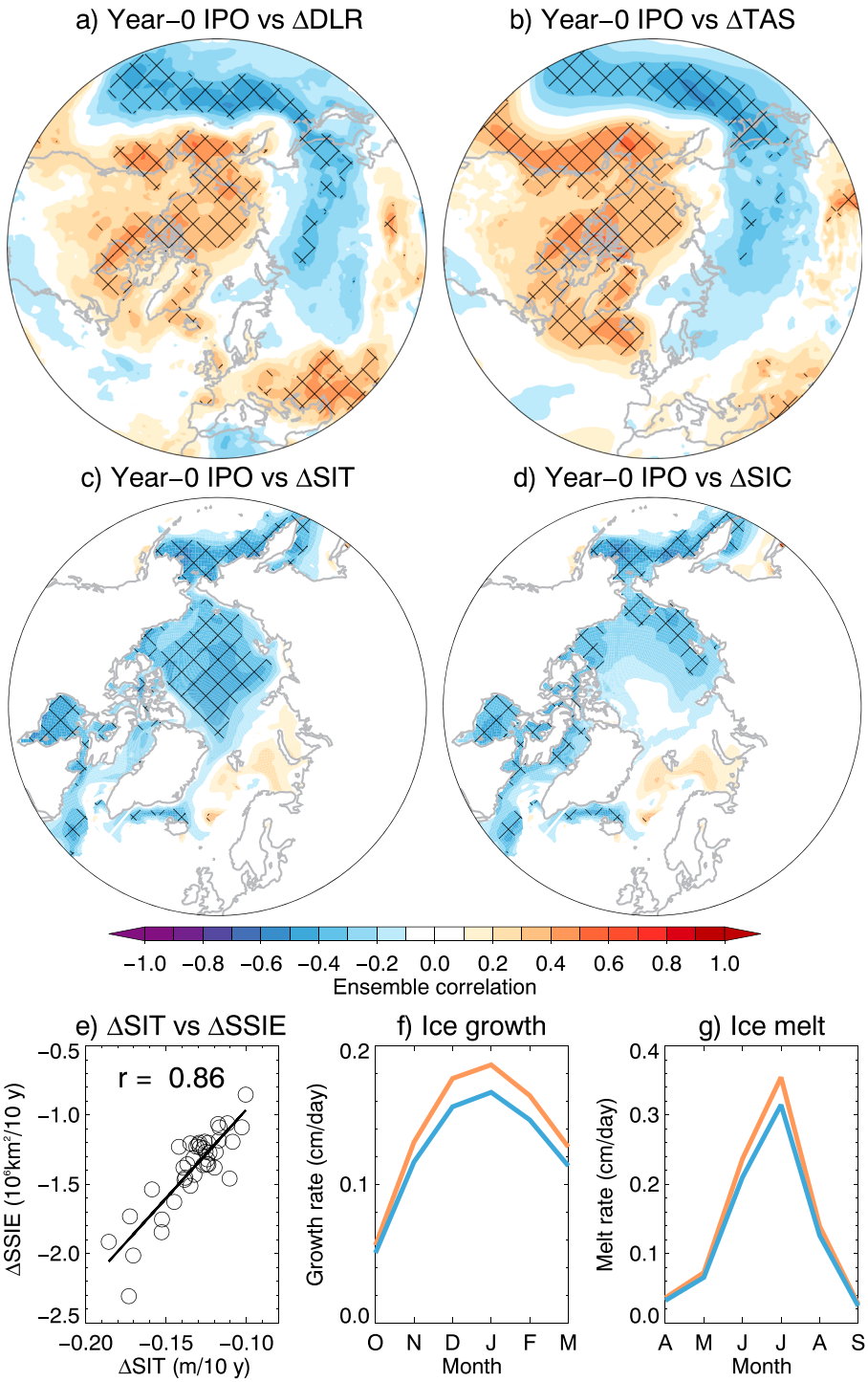

Figure 3. Interdecadal Pacific Oscillation (IPO) phase transition affects the Arctic. (a) Ensemble correlation between the IPO index in year 0 and the cold season (October–March) downward longwave radiation (DLR) trend in each trajectory. Black hatching shows statistical significance at the 95% confidence level ($p < 0.05$). (b–d) As (a), but for the correlation between the IPO index in year 0 and the cold season (b) near-surface air temperature (TAS) trend, (c) sea-ice thickness (SIT) trend, and (d) sea-ice concentration (SIC) trend. In (a–d), the sign of the correlations has been reversed to display patterns linked to negative IPO in year 0. (e) Relationship between the cold season Arctic-mean sea-ice thickness trend and September sea-ice extent (SSIE) trend in each trajectory. The black line denotes the linear best fit. (f) Monthly and Arctic mean sea ice growth rates (sum of congelation, frazil ice growth, and snow-ice formation), averaged over trajectories starting in negative IPO ($< -0.9\sigma$; blue) and positive IPO ($>0.9\sigma$; orange). (g) As (f), but for sea-ice melt rates (sum of top, bottom, and lateral melt).

negative IPO compared to those starting in the positive IPO (Figures 3f and 3g). Thus, the faster SSIE decline in the former is caused by IPO-related reductions in sea-ice growth rather than enhanced summer melting.

Winter preconditioning has been previously shown to be an important driver of interannual fluctuations of SSIE (e.g., Park et al., 2018; Rigor et al., 2002; Williams et al., 2016) and has contributed to recent SSIE trends. Recent extreme SSIE minima have been linked to thinner winter ice cover that is more vulnerable to summer melt, driven in part by internal atmospheric variability (predominantly positive Arctic Oscillation) in the late 1980s through mid-1990s (Lindsay & Zhang, 2005; Rigor & Wallace, 2004). Holland and Stroeve (2011) showed that the variance of SSIE explained by winter sea-ice precursors, such as winter ice thickness, increases during the transition to a seasonally ice-covered Arctic. We propose that IPO-induced preconditioning is a proximal cause for an earlier occurrence of an ice-free Arctic in trajectories starting in the negative IPO phase than those starting in the positive IPO phase. However, it is likely that other processes also play a role, for example, tropically induced high-latitude circulation changes in summer, as suggested by other studies (Ding et al., 2019; Meehl et al., 2018).

4. Discussion

Our study is not the first to suggest a specific role for Pacific Ocean variability in modulating projections of 21st century Arctic sea-ice loss. Wettstein and Deser (2014) examined a large ensemble of the Community Climate System Model version 3 (a predecessor to CESM1) and showed that tropical Pacific Ocean variability modulated SSIE trends over the period 2020–2059. Higher rates of projected SSIE loss were found to be associated with an atmospheric Rossby wave train over the Pacific, which closely resembles that found to be connected to the IPO in this study (cf. their Figures 11 and 12 and our Figure 3).

Meehl et al. (2018) suggest a role for Pacific decadal variability in the accelerated Arctic winter sea-ice loss from 2000 to 2014. Interestingly, these authors conclude that reduced convection over the tropical Pacific, associated with the negatively trending IPO from 2000 to 2014, contributed to enhanced winter Arctic sea-ice loss. On the face of it, this result seems at odds with our finding that the transition from negative to positive IPO favors enhanced winter sea-ice loss. A likely explanation for this apparent discrepancy is that winter sea-ice loss from 2000 to 2014 occurred primarily in the Barents Sea, whereas future winter sea-ice loss is projected to be more widespread. The impact of the IPO on sea-ice varies by geographic location. Indeed, Figures 3c and 3d suggests that the transition from negative to positive IPO *slows* sea-ice loss in the Barents Sea. Therefore, our results do not contradict a contributing role of the negatively trending IPO in the accelerated winter sea-ice loss from 2000 to 2014 in the Barents Sea. They suggest, however, that in the future, IPO-associated sea-ice changes in the Pacific sector may dominate over opposite-signed sea-ice changes in the Atlantic sector.

Pacific Ocean variability appears to have played a key role in the accelerated Arctic warming during the early twentieth century (Svendson et al., 2018; Tokinaga et al., 2017). Svendson et al. (2018) concluded that during the early twentieth century, the Pacific Decadal Oscillation transitioned to a positive phase with a concomitant deepening of the Aleutian Low, which warmed the Arctic by poleward low-level advection of extratropical air, which is highly consistent with our results.

5. Conclusions

We have examined the influence of internal climate variability on the trajectory to, and timing of, a seasonally ice-free Arctic Ocean. In the CESM1-LE, the speed of transition from present-day September ice extent to an ice-free state is modulated by concomitant changes in the IPO, which are partially predictable from the IPO phase at the start of the trajectory. More specifically, trajectories starting in the negative IPO phase are characterized by a subsequent positive IPO trend, strengthening of the Aleutian Low, increased poleward heat and moisture transport, and an earlier emergence of an ice-free Arctic. Conversely, trajectories starting in the positive IPO phase are characterized by a subsequent negative IPO trend, weakening of the Aleutian Low, reduced poleward heat and moisture transport, and a later emergence of an ice-free Arctic. Trajectories starting in the positive IPO phase become ice-free 7 years sooner than those starting in the negative IPO phase, on average. This 7-year difference equates to one third of the total uncertainty due to internal variability in the time of emergence of an ice-free Arctic in the CESM1-LE. We are cognisant that our results are based on simulations from a single model and only one possible emissions scenario and thus must be

interpreted with a degree of caution. It remains for future work to determine whether other models and scenarios exhibit similar behavior.

Our results suggest that the current IPO state may provide predictive information on the likelihood of faster, or slower, sea-ice loss over the coming decade(s). The observed IPO began to transition away from its peak negative phase in the past few years (Figure 1d). If the IPO continues to transition toward its positive phase, as is predicted by decadal IPO forecasts (Meehl, Hu, et al., 2016), our results suggest that there is increased likelihood of accelerated loss of sea-ice over the coming decade or two, compared to if the IPO was trending downward, and an increased risk of witnessing an ice-free Arctic within the next 20–30 years. We note, of course, that the IPO is not the only factor that will modulate the rate of Arctic sea-ice loss in coming decades. Near-future changes in sea-ice will also depend on external forcing, including the rate of anthropogenic emissions of greenhouse gases (Jahn, 2018) and aerosols (Gagne et al., 2015).

Acknowledgments
The authors thank Ben Henley and three anonymous reviewers for their feedback. James Screen received funding from the Natural Environment Research Council (NE/N018486/1) and the Leverhulme Trust (PLP-2015-215). The National Science Foundation supports NCAR. Data are freely available at the following repositories: CESM1 Large Ensemble, http://www.cesm.ucar.edu/projects/community-projects/LENS/data-sets.html; NOAA ERSST version 5, https://www1.ncdc.noaa.gov/pub/data/cmb/ersst/v5/netcdf/; and NSIDC Sea Ice Index, ftp://sidads.colorado.edu/DATASETS/NOAA/G02135/.

References

Day, J., Hargreaves, J., Annan, J., & Abe-Ouchi, A. (2012). Sources of multi-decadal variability in Arctic sea ice extent. *Environmental Research Letters*, *7*(3), 034011. https://doi.org/10.1088/1748-9326/7/3/034011

Ding, Q., Schwieger, A., L'Heureux, M., Battisti, D., Po-Chedley, S., Johnson, N., et al. (2017). Influence of high-latitude atmospheric circulation changes on summertime Arctic Sea ice. *Nature Climate Change*, *7*(4), 289–295. https://doi.org/10.1038/nclimate3241

Ding, Q., Schwieger, A., L'Heureux, M., Steig, E., Battisti, D., Johnson, N., et al. (2019). Fingerprints of internal drivers of Arctic sea ice loss in observations and model simulations. *Nature Geoscience*, *12*(1), 28–33. https://doi.org/10.1038/s41561-018-0256-8

Fetterer, F., Knowles, K., Meier, W., Savoie, M., & Windnagel, A. (2017). Sea ice index, Version 3. Boulder, CO: National Snow and Ice Data Center. https://doi.org/10.7265/N5K072F8

Gagne, M.-E., Gillett, N., & Fyfe, J. (2015). Impact of aerosol emission controls on future Arctic sea ice cover. *Geophysical Research Letters*, *42*, 8481–8488. https://doi.org/10.1002/2015GL065504

Germe, A., Chevallier, M., Salas y Melia, D., Sanchez-Gomez, E., & Cassou, C. (2014). Interannual predictability of Arctic sea ice in a global climate model: Regional contrasts and temporal evolution. *Climate Dynamics*, *43*, 2519–2538.

Gong, T., Feldstein, S., & Lee, S. (2017). The role of downward infrared radiation in the recent Arctic winter warming trend. *Journal of Climate*, *30*(13), 4937–4949. https://doi.org/10.1175/JCLI-D-16-0180.1

Guemas, V., Blanchard-Wrigglesworth, E., Chevallier, M., Day, J., Deque, M., Doblas-Reyes, F., et al. (2016). A review on Arctic sea-ice predictability and prediction on seasonal to decadal time-scales. *Quarterly Journal of the Royal Meteorological Society*, *142*, 546–561.

Hawkins, E., & Sutton, R. (2012). Time of emergence of climate signals. *Geophysical Research Letters*, *39*, L01702. https://doi.org/10.1029/2011GL050087

Henley, B., Gergis, J., Karoly, D., Power, S., Kennedy, J., & Folland, C. (2015). A Tripole Index for the Interdecadal Pacific Oscillation. *Climate Dynamics*, *45*(11-12), 3077–3090. https://doi.org/10.1007/s00382-015-2525-1

Holland, M., & Stroeve, J. (2011). Changing seasonal sea ice predictor relationships in a changing Arctic climate. *Geophysical Research Letters*, *38*, L18501. https://doi.org/10.1029/2011GL049303

Huang, B., Thorne, P., Banzon, V., Boyer, T., Chepurin, G., Lawrimore, J., et al. (2017). Extended Reconstructed Sea Surface Temperature version 5 (ERSSTv5): Upgrades, validations, and intercomparisons. *Journal of Climate*, *30*(20), 8179–8205. https://doi.org/10.1175/JCLI-D-16-0836.1

Jahn, A. (2018). Reduced probability of ice-free summers for 1.5 °C compared to 2 °C warming. *Nature Climate Change*, *8*(5), 409–413. https://doi.org/10.1038/s41558-018-0127-8

Jahn, A., Kay, J., Holland, M., & Hall, D. (2016). How predictable is the timing of a summer ice-free Arctic? *Geophysical Research Letters*, *43*, 9113–9120. https://doi.org/10.1002/2016GL070067

Kay, J., Deser, C., Phillips, A., Mai, A., Hannay, C., Strand, G., et al. (2015). The Community Earth System Model (CESM) Large Ensemble project: A community resource for studying climate change in the presence of internal climate variability. *Bulletin of the American Meteorological Society*, *96*(8), 1333–1349. https://doi.org/10.1175/BAMS-D-13-00255.1

Kay, J., Holland, M., & Jahn, A. (2011). Inter-annual to multi-decadal Arctic Sea ice extent trends in a warming world. *Geophysical Research Letters*, *38*, L15708. https://doi.org/10.1029/2011GL048008

Koenigk, T., Beatty, C., Caian, M., Doscher, R., & Wyser, K. (2012). Potential decadal predictability and its sensitivity to sea ice albedo parameterization in a global coupled model. *Climate Dynamics*, *38*(11-12), 2389–2408. https://doi.org/10.1007/s00382-011-1132-z

Lee, S., Gong, T., Feldstein, S., Screen, J., & Simmonds, I. (2017). Revisiting the cause of the 1989–2009 Arctic surface warming using the surface energy budget: Downward infrared radiation dominates the surface fluxes. *Geophysical Research Letters*, *44*, 10,654–10,661. https://doi.org/10.1002/2017GL075375

Lee, S., Wang, C., & Mapes, B. (2009). A simple atmospheric model of the local and teleconnection responses to tropical heating anomalies. *Journal of Climate*, *22*(2), 272–284. https://doi.org/10.1175/2008JCLI2303.1

Lindsay, R., & Zhang, J. (2005). The thinning of Arctic Sea ice, 1988-2003: Have we passed a tipping point? *Journal of Climate*, *18*(22), 4879–4894. https://doi.org/10.1175/JCLI3587.1

Mahlstein, I., & Knutti, R. (2012). September Arctic sea ice predicted to disappear near 2 °C warming above present. *Journal of Geophysical Research*, *117*, D06104. https://doi.org/10.1029/2011JD0016709

Meehl, G., Arblaster, J., Bitz, C., Chung, C., & Teng, H. (2016). Antarctic sea-ice expansion between 2000 and 2014 driven by tropical Pacific decadal climate variability. *Nature Geoscience*, *9*(8), 590–595. https://doi.org/10.1038/ngeo2751

Meehl, G., Chung, C., Arblaster, J., Holland, M., & Bitz, C. (2018). Tropical decadal variability and the rate of Arctic sea ice decrease. *Geophysical Research Letters*, *45*, 11,326–11,333. https://doi.org/10.1029/2018GL079989

Meehl, G., Hu, A., & Teng, H. (2016). Initialized decadal prediction for transition to positive phase of the Interdecadal Pacific Oscillation. *Nature Communications*, *7*(1), 11718. https://doi.org/10.1038/ncomms11718

Newman, M., Alexander, M., Ault, T., Cobb, K., Deser, C., Di Lorenzo, E., et al. (2016). The Pacific Decadal Oscillation, revisited. *Journal of Climate*, *29*(12), 4399–4427. https://doi.org/10.1175/JCLI-D-15-0508.1

Niederdrenk, A. L., & Notz, D. (2018). Arctic sea ice in a 1.5 °C warmer world. *Geophysical Research Letters*, *45*, 1963–1971. https://doi.org/10.1002/2017GL076159

Notz, D., & Stroeve, J. (2016). Observed Artic sea-ice loss directly follows anthropogenic CO_2 emission. *Science*, *354*(6313), 747–750. https://doi.org/10.1126/science.aag2345

Notz, D., & Stroeve, J. (2018). The trajectory towards a seasonally ice-free Arctic Ocean. *Current Climate Change Reports*, *4*(4), 407–416. https://doi.org/10.1007/s40641-018-0113-2

Park, H., Stewart, A., & Son, J. (2018). Dynamic and thermodynamic impacts of the winter Arctic Oscillation on summer sea ice extent. *Journal of Climate*, *31*(4), 1483–1497. https://doi.org/10.1175/JCLI-D-17-0067.1

Petty, A., Holland, M., Bailey, D., & Kurtz, N. (2018). Warm Arctic, increased winter sea ice growth? *Geophysical Research Letters*, *45*, 12,922–12,930. https://doi.org/10.1029/2018GL079223

Purich, A., England, M., Cai, W., Chikamoto, Y., Timmermann, A., Fyfe, J., et al. (2016). Tropical Pacific SST drivers of recent Antarctic sea ice trends. *Journal of Climate*, *29*(24), 8931–8948. https://doi.org/10.1175/JCLI-D-16-0440.1

Rigor, I., & Wallace, J. (2004). Variations in the age of Arctic sea-ice and summer sea-ice extent. *Geophysical Research Letters*, *31*, L09401. https://doi.org/10.1029/2004GL019492

Rigor, I., Wallace, J., & Colony, R. (2002). Response of sea ice to the Arctic Oscillation. *Journal of Climate*, *15*(18), 2648–2663. https://doi.org/10.1175/1520-0442(2002)015<2648:ROSITT>2.0.CO;2

Rosenblum, E., & Eisenman, I. (2016). Faster Arctic sea ice retreat in CMIP5 than in CMIP3 due to volcanoes. *Journal of Climate*, *29*(24), 9179–9188. https://doi.org/10.1175/JCLI-D-16-0391.1

Rosenblum, E., & Eisenman, I. (2017). Sea ice trends in climate models only accurate in runs with biased global warming. *Journal of Climate*, *30*(16), 6265–6278. https://doi.org/10.1175/JCLI-D-16-0455.1

Schneider, D., & Deser, C. (2017). Tropically driven and externally forced patterns of Antarctic sea ice change: Reconciling observed and modelled trends. *Climate Dynamics*, *50*, 4599–4618.

Screen, J. (2018). Arctic sea ice at 1.5 and 2 °C. *Nature Climate Change*, *8*(5), 362–363. https://doi.org/10.1038/s41558-018-0137-6

Screen, J., & Simmonds, I. (2010). Increasing fall-winter energy loss from the Arctic Ocean and its role in Arctic temperature amplification. *Geophysical Research Letters*, *37*, L16797. https://doi.org/10.1029/2010GL044136

Screen, J., & Williamson, D. (2017). Ice-free Arctic at 1.5 °C? *Nature Climate Change*, *7*(4), 230–231. https://doi.org/10.1038/nclimate3248

Sigmond, M., Fyfe, J., & Swart, N. (2018). Ice-free Arctic projections under the Paris Agreement. *Nature Climate Change*, *8*(5), 404–408. https://doi.org/10.1038/s41558-018-0124-y

Stroeve, J., Kattsov, V., Barrett, A., Serreze, M., Pavlova, T., Holland, M., & Meier, W. (2012). Trends in Arctic sea ice extent from CMIP5, CMIP3 and observations. *Geophysical Research Letters*, *39*, L16502. https://doi.org/10.1029/2012GL052676

Stroeve, J., & Notz, D. (2018). Changing state of Arctic sea ice across all seasons. *Environmental Research Letters*, *13*(10). https://doi.org/10.1088/1748-9326/aade56

Stroeve, J., Schroder, D., Tsamados, M., & Feltham, D. (2018). Warm winter, thin ice? *The Cryosphere*, *12*(5), 1791–1809. https://doi.org/10.5194/tc-12-1791-2018

Svendson, L., Keenlyside, N., Bethhke, I., Gao, Y., & Omrani, N.-E. (2018). Pacific contribution to the early twentieth-century warming in the Arctic. *Nature Climate Change*, *8*(9), 793–797. https://doi.org/10.1038/s41558-018-0247-1

Swart, N., Fyfe, J., Hawkins, E., Kay, J., & Jahn, A. (2015). Influence of internal variability on Arctic sea-ice trends. *Nature Climate Change*, *5*(2), 86–89. https://doi.org/10.1038/nclimate2483

Thomson, S., & Vallis, G. (2018a). Atmospheric response to SST anomalies. Part I: Background-state dependence, teleconnections, and local effects in winter. *Journal of the Atmospheric Sciences*, *75*(12), 4107–4124. https://doi.org/10.1175/JAS-D-17-0297.1

Thomson, S., & Vallis, G. (2018b). Atmospheric response to SST anomalies. Part II: Background-state dependence, teleconnections, and local effects in summer. *Journal of the Atmospheric Sciences*, *75*(12), 4125–4138. https://doi.org/10.1175/JAS-D-17-0298.1

Tokinaga, H., Xie, S.-P., & Mukougawa, H. (2017). Early 20th-century Arctic warming intensified by Pacific and Atlantic multidecadal variability. *Proceedings of the National Academy of Sciences of the United States of America*, *114*(24), 6227–6232. https://doi.org/10.1073/pnas.1615880114

Trenberth, K., & Hurrell, J. (1994). Decadal atmosphere-ocean variations in the Pacific. *Climate Dynamics*, *9*(6), 303–319. https://doi.org/10.1007/BF00204745

Wettstein, J., & Deser, C. (2014). Internal variability in projections of twenty-first-century Arctic sea ice loss: Role of the large-scale atmospheric circulation. *Journal of Climate*, *27*(2), 527–550. https://doi.org/10.1175/JCLI-D-12-00839.1

Williams, J., Tremblay, B., Newton, R., & Allard, R. (2016). Dynamic preconditioning of the minimum September sea-ice extent. *Journal of Climate*, *29*(16), 5879–5891. https://doi.org/10.1175/JCLI-D-15-0515.1

Yang, C.-Y., Liu, J., Hu, Y., Horton, R., Chen, L., & Cheng, X. (2016). Assessment of Arctic and Antarctic sea ice predictability in CMIP5 decadal hindcasts. *The Cryosphere*, *10*(5), 2429–2452. https://doi.org/10.5194/tc-10-2429-2016

Yeager, S., Karspeck, A., & Danabasoglu, G. (2015). Predicted slowdown in the rate of Atlantic sea ice loss. *Geophysical Research Letters*, *42*, 10,704–10,713. https://doi.org/10.1002/2015GL065364

Zhang, R. (2015). Mechanisms for low-frequency variability of summer Arctic sea ice extent. *Proceedings of the National Academy of Sciences of the United States of America*, *112*(15), 4570–4575. https://doi.org/10.1073/pnas.1422296112